Journal of Sound and Vibration 330 (2011) 136–152

Contents lists available at ScienceDirect

Journal of Sound and Vibration

journal homepage: www.elsevier.com/locate/jsvi

Spectral decomposition of the aerodynamic noise generated by rotating sources

Alessandro Bongiovì [1], Andrea Cattanei *

DIMSET-Università di Genova, via Montallegro, 1, I-16145 Genova, Italy

ARTICLE INFO

Article history:
Received 4 March 2009
Received in revised form
21 July 2010
Accepted 29 July 2010
Handling Editor: P. Joseph
Available online 23 August 2010

ABSTRACT

A method is posed for separating the noise emitted by an aerodynamic source from propagation effects using spectral decomposition. This technique is applied to the power spectra of a fan measured at several rotational speeds. Although it has been conceived for rotating sources as turbomachinery rotors, the method may be easily applied to low speed stationary sources such as jets and flows in stators and about isolated airfoils.

Based on the similarity theory, a clear description of the structure of the power spectrum of the received noise is given and the effect of rotational speed variations is considered as a means to obtain a data set suitable to perform the spectral decomposition. The problem is analyzed in order to clarify possibilities and limitations of the method and then an algorithm is presented which is based on the solution of the derived equations. Particular care is devoted to both the numerical details and the operative aspects.

The validation of the algorithm is performed by means of numerically generated input data. Next, in order to verify the ability of the method in separating scattered from emitted sound, an automotive cooling fan has been tested in the DIMSET hemi-anechoic room in a free-field configuration and with a shielded microphone. These two apparently distinct spectra collapse to within less than 2 dB after the spectral decomposition has been performed. The tests prove the ability of the method despite the modest quantity of input data.

1. Introduction

The aerodynamic noise generated by the interaction of solid bodies with a fluid flow usually results from the composition of two distinct phenomena: the generation mechanism, which depends on the flow velocity, and the propagation effects, which depend on both the geometry and the acoustic properties of the surrounding environment. For low-speed fans, some typical instances are the reorganization of the acoustic waves taking place when a fan is inserted inside a duct and the reflection, the scattering and the diffraction due to solid bodies within the surrounding environment. Often, the propagation effects are considered extraneous and one is interested in obtaining their measured acoustic pressure contribution. In other situations eliminating the propagation effects allows to study the noise generation mechanism or to determine the acoustic signature.

* Corresponding author. Tel.: +39 010 353 2445; fax: +39 010 353 2566.
E-mail addresses: alessandro.bongiovi@it.abb.com (A. Bongiovì), Andrea.Cattanei@unige.it (A. Cattanei).
[1] Present address: ABB Energy Automation SPA, via Hermada, 6, I-16153 Genova, Italy.

0022-460X/$ - see front matter © 2010 Elsevier Ltd. All rights reserved.
doi:10.1016/j.jsv.2010.07.024

Nomenclature

a_0	speed of sound
a_{mn}	element of the coefficient matrix of Eq. (31)
A_{ln}	element of the coefficient matrix of Eq. (34)
$b_{i,k}$	weighting coefficient in Eqs. (26) and (30)
b_m	element of the known vector in Eq. (31)
B_l	element of the known vector in Eq. (34)
$c_{i,k}$	weighting coefficient in Eqs. (26) and (30)
C, C_1, C_2, C_3	constants in Eqs. (11–17) and (21)
D	tip diameter of the rotor
$\overline{D}$	directivity function
e	error
E	norm of the error
f	frequency
F	source spectral distribution function
$\Im$	non-dimensional function in Eq. (1)
g	non-dimensional function of Re
G	propagation function
He	Helmholtz number
K	function in Eqs. (16) and (17), K=*const* in present work
M	number of rotational speeds
Ma	Mach number at the rotor tip
N	number of discrete frequencies, number of equations and number of unknowns
n	rotational speed (rev/min)
OASPL	overall SPL, 20 μPa
p	acoustic pressure
p_0	ambient static pressure
p_{out}	static pressure at the fan discharge
p_{ref}	reference acoustic pressure, 20 μPa
Q	volume flow rate
r	distance from the rotor center
Re	Reynolds number at the rotor tip
SPL	sound pressure level, 20 μPa
S_{pp}	power spectral density of the acoustic pressure
S_{random}	numerically generated random error
St	Strouhal number based on the rotational frequency
$T_{i,k}$	right-hand side term in Eq. (29)
x_n	element of the solution vector of Eq. (33)
x_n^*	best approximation of x_n
y_n	element of the approximate solution vector of Eq. (33)

Greek letters

α	Mach number exponent in Eq. (9)
β	Reynolds number exponent in Eq. (9)
γ	parameter related to the "frequency period" in Eq. (40)
Γ	level of the function G
$\overline{\Gamma}$	average value of Γ
Δf	frequency resolution
ΔSt	Strouhal number resolution
$\Delta\Omega$	rotational speed resolution
Θ	inclination angle
λ	wavelength
ν	kinematic viscosity
ρ_0	ambient air density
φ	$=8Q/\pi\Omega D^3$, flow coefficient
Φ	level of the function F
ψ	$=8(p_{out}-p_0)/\rho_0(\Omega D)^2$, pressure coefficient
Ω	rotational speed (rad/s)

Subscripts

an	related to SPL, Φ, Γ resulting from analytical expressions
comp	related to SPL, Φ, Γ resulting from the spectral decomposition
eq	related to the equations
ff	related to free-field conditions and to measurements in the free-field configuration
i	related to the ith value of f
I	value of i in the constant St interpolation
k	related to the kth value of Ω
m	related to the generic equation
max	maximum value in the St range
meas	related to measured SPL power spectra
min	minimum value in the St range
n	related to the generic unknown in Eq. (31)
prop	related to the presence of propagation effects
real	related to realistic signals
sh	related to measurements with shielded microphone
un	related to the unknowns
α	related to Φ and Γ values obtained with a generic α value
0	related to the ambient conditions and to α=0

To this regard, the so-called spectral decomposition is a typical instance: the flow velocity is varied under kinematic similarity conditions so that the generation mechanism changes its time scale without affecting the time scale of the propagation mechanism. The comparison of the SPL power spectra measured at different speeds should allow to separate the two effects, but this operation requires the knowledge of the basic analytical structure of the received noise and, obviously, the availability of a suitable algorithm.

The spectral decomposition has been first employed by Weidemann [1] and Neise and Barsikow [2] but it has been extensively used and deepened by a group of researchers at the Pennsylvania State University (Mongeau et al. [3,4], Bent and McLaughlin [5], and Tetu et al. [6]), by Mongeau and Quinlan [7], and by Stephens and Morris [8]. All of the latter authors succeeded in employing the spectral decomposition for characterizing the sound generation properties of axial and centrifugal turbomachines. In Refs. [5,8,9] some practical and theoretical aspects of the employed methods are treated and different algorithms are suggested together with some enhancements to them. Nevertheless the general properties of the problem have not been thoroughly treated and limited information about the developed algorithm has been provided. The

main reason for this is that the above mentioned works were aimed at studying a specific physical phenomenon rather than at analyzing a specific method. The main aim of present work is providing a deep description of the developed algorithm and related problems.

An important aspect is the fact that, due to the properties of the physical phenomenon, the resulting mathematical problem is ill-posed and underdetermined. This complicates the development of a suitable algorithm, from both the theoretical and the numerical points of view. Even an effective algorithm cannot change the nature of a phenomenon and thus the underdeterminacy remains and the obtained solution is just a mere mathematical one. In order to obtain the actual solution further physical information is required. This aspect goes beyond the main purpose of the present work and, although some related considerations of general usefulness are reported, it is not thoroughly treated in the following.

The spectral decomposition method will be treated with reference to turbomachinery rotors, in order to describe the basic theory and to study the developed algorithm. However, no specific phenomenon is studied and, if the basic assumptions hold, the application to the aerodynamic noise generated by non-rotating sources is straightforward.

2. Theoretical background

2.1. Acoustic similarity for turbomachinery rotors

Let us consider a fan rotor radiating aerodynamic noise and a receiver located in the acoustic far field at a distance r from the rotor center. Assuming that the rotational speed Ω is sufficiently low for the flow to be considered incompressible, based on the similarity theory, see for instance Blake [10], a quite general expression of the power spectral density S_{pp} of the received acoustic pressure p is given by

$$S_{\mathrm{pp}}(f,\Omega,D,r,\Theta,\varphi)=\rho_0{}^2\Omega^3D^4\frac{1}{(r/D)^2}\Im(St,He,Re,r/d,\Theta,\varphi)\overline{D}(\Theta) \tag{1}$$

where f is the frequency, ρ_0 is the air density, D is the tip diameter of the rotor, and $\overline{D}(\boldsymbol{\Theta})$ is the directivity function, dependent on the inclination angle Θ. $\Im$ is a non-dimensional function of the following non-dimensional parameters:

$$\text{Strouhal number}\quad St=\frac{2\pi f}{\Omega} \tag{2}$$

$$\text{Helmholtz number}\quad He=\frac{fD}{a_0} \tag{3}$$

$$\text{Reynolds number}\quad Re=\frac{\Omega D^2}{2\nu} \tag{4}$$

$$\text{flow coefficient}\ \varphi=\frac{8Q}{\pi\Omega D^3} \tag{5}$$

where a_0 is the speed of sound, ν is the kinematic viscosity, and Q is the volume flow rate. Note that the blade tip Mach number may be expressed as

$$Ma=\frac{\Omega D}{2a_0}=\pi\frac{He}{St} \tag{6}$$

All quantities are expressed in SI units. In all the equations Ω will be expressed in rad/s and only in the practical examples the rotational speed n=60Ω/2π, expressed in rev/min, will be used. S_{pp} is strictly linked to the sound pressure level in the frequency band $f-\Delta f/2$, $f+\Delta f/2$:

$$\mathrm{SPL}(f,\Omega,D,r,\Theta,\varphi)=10\log_{10}\frac{\int_{f-\Delta f/2}^{f+\Delta f/2}S_{\mathrm{pp}}(f,\Omega,D,r,\Theta,\varphi)\,\mathrm{d}f}{p_{\mathrm{ref}}^2} \tag{7}$$

with p_{ref}=20 μPa. When considering a narrow band spectrum, Δf is small and Eq. (7) may be approximated as

$$\mathrm{SPL}(f,\Omega,D,r,\Theta,\varphi)\cong 10\log_{10}\frac{S_{pp}(f,\Omega,D,r,\Theta,\varphi)\Delta f}{p_{\mathrm{ref}}^2} \tag{8}$$

The function $\Im$ has often a relatively simple structure. For instance, in a study of the noise generated by centrifugal turbomachines Neise and Barsikow [2] found that Eq. (1) may be simplified to a form equivalent to

$$S_{\mathrm{pp}}(f,\Omega,D,r,\Theta,\varphi)=\frac{\rho_0^2\Omega^3D^6}{r^2}Ma^{\alpha}Re^{\beta}F^2(St,\varphi)G^2\left(He,\frac{r}{D},\Theta\right)\overline{D}(\Theta) \tag{9}$$

that is

$$\Im\left(St,He,Re,\frac{r}{D},\Theta,\varphi\right)=Ma^{\alpha}Re^{\beta}F^2(St,\varphi)G^2\left(He,\frac{r}{D},\Theta\right)\overline{D}(\Theta)$$

$F(St,\varphi)$ is a non-dimensional source spectral distribution function which depends on the pressure and velocity fluctuations within the flow region. It is independent of the propagation effects which are included in the group $Ma^{\alpha}G^2(He,r/D,\Theta)\ \overline{D}(\Theta)$. $G(He,r/D,\Theta)$ is the non-dimensional acoustic frequency response function (in the following the "propagation function") which depends on the geometry and on the acoustic properties of the whole system. The term Ma^{α} is related to the radiation efficiency and α depends on both the active noise generation mechanism and the acoustic compactness of the source. The structure of Eq. (9) may be obtained solving the Helmholtz equation by means of the Green's function method thus allowing to identify the different contributions to the propagation effects (basically radiation efficiency, near field effects and boundary conditions). These aspects are deepened in Mongeau et al. [4], Stephens and Morris [8], and Blake [10].

Different kinds of noise generation mechanisms scaling with different powers of Ma may be simultaneously present resulting in $\alpha=\alpha(St)$, Bent and McLaughlin [5], Stephens and Morris [8], Quinlan and Krane [12]. This is explicitly taken into account by the formulation described in Ref. [8]. For the sake of simplicity, in the present work α is considered to be constant, but, as shown hereinafter, the extension to the case $\alpha=\alpha(St)$ is straightforward.

Other difficulties may stem from the structure of the noise generated by a single mechanism. As an example, for the trailing edge noise generated by axial flow fans and isolated airfoils, Blake [10] and Brooks et al. [11] suggested a more complex structure of $\Im$ which may be rearranged to yield $\Im(St,He,Re,\varphi)=Mag^2(Re)F^2[Stg(Re),\varphi]G^2(He)\overline{D}(\Theta)$. In such a case $\Im$ could not be split in a part dependent on St multiplied by a part dependent on He and the application of the present theory would be badly affected. Fortunately, in turbomachines the influence of Re on the generated noise is often weak and thus Eq. (9) applies with $\beta=0$. This assumption has been confirmed or directly employed by Neise and Barsikow [2], Mongeau et al. [3], Bent and McLaughlin [5], and Stephens and Morris [8] and allows to separate the effects of St and He. Thus, if $\beta=0$, substituting Eqs. (6) and (9) in Eq. (8) yields

$$\begin{aligned}\mathrm{SPL}(f,\Omega,D,r,\Theta,\varphi)=10\log_{10}\left[\frac{\rho_0^2\Delta f}{r^2p_{\mathrm{ref}}^2}\overline{D}(\Theta)\right]+10\log_{10}(\Omega^3D^6)+10\log_{10}Ma^{\alpha}\\+20\log_{10}F(St,\varphi)+20\log_{10}G(He,r/D,\Theta)\end{aligned}\tag{10}$$

If the receiver position is fixed, i.e. both r and Θ are constant, Eq. (10) may be further rearranged in any of the following forms:

$$\mathrm{SPL}(f,\Omega,D,\varphi)=10\log_{10}(\Omega^{3+\alpha}D^{6+\alpha})+\Phi(St,\varphi)+\Gamma(He)+C_1(\alpha)\tag{11}$$

$$\mathrm{SPL}(f,\Omega,D,\varphi)=10\log_{10}(\Omega^3D^6)+[\Phi(St,\varphi)-10\log_{10}]+[\Gamma(He)+10\log_{10}He^{\alpha}]+C_2(\alpha)\tag{12}$$

where $\Phi=20\log_{10}F$, $\Gamma=20\log_{10}G$, $C_1(\alpha)=10\log_{10}[\rho_0^2\Delta f\overline{D}(\Theta)/2^{\alpha}a_0^{\alpha}r^2p_{\mathrm{ref}}^2]$ and $C_2(\alpha)=10\log_{10}[\pi^{\alpha}\rho_0^2\Delta f/\overline{D}(\Theta)/r^2p_{\mathrm{ref}}^2]$. For an ideal open rotor (i.e. a point source) operating in free-field conditions (i.e. $\Gamma\equiv0$) S_{pp} depends on f through St only and, if $\alpha=$const, the frequency integration of Eq. (9) yields the following expression of the overall SPL:

$$\mathrm{OASPL}(\Omega,D,\varphi)=10\log_{10}\frac{\int_0^{\infty}S_{pp}(f)\,\mathrm{d}f}{p_{\mathrm{ref}}^2}=C_3(\varphi)+10\log_{10}(\Omega^{4+\alpha}D^{6+\alpha})\tag{13}$$

with

$$C_3(\varphi)=10\log_{10}\left[\frac{\rho_0^2}{2^{\alpha}\pi r^2a_0^{\alpha}p_{\mathrm{ref}}^2}\overline{D}(\Theta)\right]+10\log_{10}\int_0^{+\infty}F^2(St,\varphi)\,\mathrm{d}St$$

Eqs. (11) and (13) provide the low Mach number dependence of SPL and OASPL on Ω under kinematic similarity conditions. Eqs. (11) and (12) are the base of the present work and may be rewritten in the following forms:

$$\Phi(St,\varphi)+\Gamma(He)=\mathrm{SPL}(f,\Omega,D,\varphi)-10\log_{10}(\Omega^{3+\alpha}D^{6+\alpha})-C_1(\alpha)\tag{14}$$

$$\Phi(St,\varphi)+\Gamma(He)=\mathrm{SPL}(f,\Omega,D,\varphi)-10\log_{10}(\Omega^3D^6)+10\log_{10}St^{\alpha}-10\log_{10}He^{\alpha}-C_2(\alpha)\tag{15}$$

On the left hand sides of Eqs. (14) and (15) there are the unknown functions Φ and Γ, while on the right hand sides only known quantities are present. Eq. (14) implies that, if the propagation effects included in Γ are negligible, the SPL spectra generated by a rotor of fixed D and rotating at variable Ω, should collapse on a single curve when scaled with $10\log_{10}\Omega^{3+\alpha}$ and plotted versus St. Together with the scaling of the OASPL, Eq. (13), this may help find the actual value of α. Given a set of experimental data, the spectral decomposition consists in separating Φ and Γ, provided that the structure given by Eq. (10) is respected; this should be verified. Unfortunately this is not sufficient for the present method to work properly since a number of practical and theoretical difficulties remain which result in an ill-posed mathematical problem. Since multiple solutions are admitted a further deepening is necessary:

(1) Once any pair of functions $\Phi(St,\varphi)$ and $\Gamma(He)$ satisfying either of Eq. (14) or (15) has been found, it is immediate to demonstrate that the pair of functions $\Phi'(St,\varphi)=\Phi(St,\varphi)+K$ and $\Gamma'(He)=\Gamma(He)-K$ also satisfies Eq. (15). In the general

case, for instance if $\alpha=\alpha(St)$, K is a function of St resulting in a wide variety of solutions. If, as in the present case, one is concerned with a single generation mechanism for which $\alpha=$const, then K may be regarded as a constant linked to the absolute levels of Φ and Γ. These levels are undetermined and only the relative trends of Φ and Γ may be determined. Although this results in an underdetermined system of equations, convergence may be reached when employing an iterative method of solution but the resulting absolute levels of $\Phi(St,\varphi)$ and $\Gamma(He)$ depend on the employed algorithm.

(2) Even in case $\alpha=$const, the α value is not unique: any α may be imposed in Eqs. (14) and (15) and for each α a different solution may be found. If the pair $\Phi_0(St,\varphi)$ and $\Gamma_0(He)$ satisfies Eq. (15) with $\alpha=0$, i.e. if $\mathrm{SPL}(f,\ \Omega,\ D,\ \varphi)-10\log_{10}(\Omega^3D^6)-C_2(0)=\Phi_0(St,\varphi)+\Gamma_0(He)$, then the pair:

$$\Phi_\alpha(St,\varphi)=\Phi_0(St,\varphi)+10\log_{10}St^\alpha+K \tag{16}$$

$$\Gamma_\alpha(He)=\Gamma_0(He)-10\log_{10}He^\alpha+[C_2(0)-C_2(\alpha)]-K \tag{17}$$

also satisfies Eq. (15) for any value of α (and obviously of K). This holds even in case $\alpha=\alpha(St)$. It may be easily demonstrated by means of the formal substitution $\Gamma=\Gamma(He,St)$ in place of $\Gamma=\Gamma(He)$ in Eq. (17), thus resulting in the term $10\log_{10}He^{\alpha(St)}$ in place of the term $10\log_{10}He^\alpha$. This last possibility will not be considered in the present work.

It has been proven that if the structure of Eq. (9) applies to the experimental data and if $\alpha=$const, any α and K may be imposed and ∞^2 solutions are possible. But, above all, the terms K, St^α, and He^α in Eqs. (16) and (17) demonstrate that K and α influence the radiated acoustic power, Eq. (13), and that, as shown by Bent and McLaughlin [5], α influences the mean slope of both Φ and Γ. Together with the scaling of the spectra, these considerations provide a physical ground for choosing both K and α: for instance any information on the high f asymptotic behavior of Φ (see for instance Blake [10] or Chase [13]) or of Γ may be of help. The application of these criteria is not restricted to low-speed fans but extends to all those phenomena to which the described theory applies. It is also clear that, no matter the value assigned to α prior to the spectral decomposition, once the latter has been performed, the resulting functions Φ and Γ may be easily modified according to Eqs. (16) and (17). Thus it is possible to comply with any K and α without performing any new spectral decomposition. This holds even in case that $\alpha=\alpha(St)$. However, the method cannot determine K and α since their indeterminacy is intrinsic to the physical problem and their estimation requires further knowledge about the properties of the source (i.e. the Mach number dependence of the noise generation mechanism) and of the propagation environment. Bent and McLaughlin [5] found K and α by means of an independent experimental evaluation of Γ: they considered it as an acoustic transfer function independent of the aerodynamic source and placed a loudspeaker of known properties at the impeller discharge. By means of a series of measurements they could evaluate the acoustic transfer function. Comparing it with the function Γ resulting from the spectral decomposition they estimated both K and α. Unfortunately, depending on the frequency range, different α values resulted and this outcome was attributed to inaccuracies in the measurements at low f or to variable scaling of the acoustic pressure with Ω. These results prove that the indeterminacy of K and α is an intrinsic feature of the physical problem and is independent of the algorithm employed to perform the spectral decomposition. Hence, their determination requires information about the involved phenomena. See Tetu et al. [6] and Quinlan and Krane [12] for further considerations about this point and Blake [10] for a general exposition of the properties of the noise mechanisms.

Although the theory has been developed for a rotating source, if the basic assumptions hold, it may be also applied to the aerodynamic noise generated in absence of rotation. This only requires substituting the specific reference velocity to the product ΩD in all the equations.

2.2. Brief description of the existing algorithms

The present study provides an extension of the works presented in [3–5], thus it is worthy to clarify that Φ and Γ equal the quantities $20\log_{10}F$ and $20\log_{10}G$ employed in Refs. [3–5], respectively, and that in the present paper St is based on the rotational frequency $\Omega/2\pi$ while in Refs. [3–5] it is based on the blade passing frequency.

Mongeau et al. [3,4] studied the noise generated by a centrifugal pump by means of a method based on seeking $\Gamma(He)$ first and then calculating $\Phi(St,\varphi)$ as the difference between the scaled SPL and Γ. The entire experimental data set $\mathrm{SPL}_{i,k}=\mathrm{SPL}(f_i,\ \Omega_k)$ is scaled with $10\log_{10}\Omega^3$ and then reorganized in subsets corresponding to a fixed value of St. Plotting these subsets against He provides a number of curves which represent shifted pieces of the function $\Gamma(He)$. They should superpose when shifted of a suitable value which is function of St and equals the increment of $\Phi(St,\varphi)$ between the corresponding St values. Unfortunately, the curves cannot perfectly superpose due to experimental errors and spurious phenomena thus causing practical complications. The authors suggest either a manual or an automated shifting of the curves.

Zhang et al. [9] studied the noise generated by a turbulent jet at variable Reynolds number. In this case there are three free parameters (St, He, Re) instead of two (St, He) and the reorganization of the experimental data set results in constant He surfaces instead of constant St curves. Γ equals the shift of the constant He surfaces which yields their best superposition. In order to determine such a shift the authors employ a least squares method based on an "ensemble average of all data available", but no further details are provided.

The above described methods are both based on a reorganization of the data set allowing to plot them as functions of non-dimensional variables and then on the shift of the resulting curves or surfaces. Automating the shifting procedure is a complicated numerical problem since both the frequency spacing and the overlapping *He* range of the curves depend on *St*. This aspect and the related problems will be faced hereinafter.

An alternative approach has been suggested by Stephens and Morris [8]. Their algorithm is based on an iterative smoothing of the non-dimensional SPL curves in the Strouhal number domain, so as to eliminate the propagation function. The method aims at "determining the small-scales features of the propagation function" and less attention is devoted to the "large-scale trends". Hence, this approach has not been followed in the present work.

3. The present method

3.1. The system of equations

The present algorithm has been developed for analyzing usual SPL power spectra for which the frequency spacing Δf and the frequency range f_1–f_N are fixed and independent of Ω, while the rotational speed spacing $\Delta\Omega$ may be chosen rather freely, usually $\Delta\Omega$=const. Thus,

$$f_i = i\Delta f, \quad i = 1,N \tag{18}$$

$$\Omega_k = \Omega_1 + (k-1)\Delta\Omega, \quad k = 1,M \tag{19}$$

This results in N evenly spaced values He_i and $N\times M$ values $St_{i,k}$, with spacing ΔSt_k function of Ω_k: $\Delta St_k = 2\pi\Delta f/\Omega_k$. In principle the unknowns are $N\times M$ values $\Phi_{i,k}$ and $N\times M$ values $\Gamma_{i,k}$, but Γ is function of *He* only and *He* is independent of Ω. Therefore,

$$\Gamma_{i,k} \equiv \Gamma_i, \quad i = 1,N \tag{20}$$

reducing the number of unknowns to $N(M+1)$. Eq. (14) yields $M\times N$ independent relations:

$$\Gamma_i + \Phi_{i,k} = \mathrm{SPL}_{i,k} - 10\log_{10}\Omega_k^{3+\alpha} - C \tag{21}$$

with $C=C_1(\alpha)+10\log_{10}D^{6+\alpha}$. A constant α value has to be assigned prior to the spectral decomposition, but then a new α may be applied to the obtained trends of Φ and Γ. A further relation is needed which represents the property of Φ of being function of *St* only. This relation should link values of Φ relative to different Ω and f and to the same *St*, but is not immediately available due to the variable spacing of *St*. The simplest way of obtaining such a relation is linking $\Phi_{i,k}$ to a value of Φ taken at Ω_{k+1} and interpolated between two suitable frequencies $f_I=I\Delta f$ and $f_{I+1}=(I+1)\,\Delta f$:

$$\Phi_{i,k} = b_{i,k}\Phi_{I,k+1} + c_{i,k}\Phi_{I+1,k+1}, \quad k = 1,M\text{-}1 \tag{22}$$

with $b_{i,k}$ and $c_{i,k}$ such that $St_{i,k} = b_{i,k}St_{I,k+1} + c_{i,k}St_{I+1,k+1}$. I may be determined imposing that

$$St_{I,k+1} \le St_{i,k} \le St_{I+1,k+1} \tag{23}$$

and $St_{I,k+1}$ may be found substituting Eq. (18) in Eq. (2):

$$St_{I,k+1} = \frac{2\pi f_I}{\Omega_{k+1}} = I\frac{2\pi f}{\Omega_{k+1}} \tag{24}$$

Substituting Eq. (24) into Eq. (23) yields

$$I \equiv I_{i,k} = \mathrm{int}\left[i\frac{\Omega_{k+1}}{\Omega_k}\right] \tag{25}$$

and thus

$$b_{i,k} = \frac{St_{I+1,k+1} - St_{i,k}}{St_{I+1,k+1} - St_{I,k+1}} = \frac{2\pi(I+1)(\Delta f/\Omega_{k+1}) - 2\pi i(\Delta f/\Omega_k)}{2\pi(\Delta f/\Omega_{k+1})} = I + 1 - i(\Omega_{k+1}/\Omega_k) \tag{26}$$

$$c_{i,k} = \frac{St_{i,k} - St_{I,k+1}}{St_{I+1,k+1} - St_{I,k+1}} = \frac{2\pi i(\Delta f/\Omega_k) 2\pi I(\Delta f/\Omega_{k+1})}{2\pi\Delta f/\Omega_{k+1}} = i(\Omega_{k+1}/\Omega_k) - I = 1 - b_{i,k} \tag{27}$$

For each value of k ranging between 1 and $M-1$, Eq. (22) yields i=1, N_k independent relations. N_k equals the maximum value of i such that $St_{i,k} \le St_{N,k+1}$:

$$N_k = \mathrm{int}\left[N\frac{\Omega_k}{\Omega_{k+1}}\right] < N \tag{28}$$

In order to reduce the number of equations to be solved simultaneously and to simplify the system of equations, Eq. (21) is calculated in k and then subtracted from the same equation calculated in k+1, thus allowing Γ_i to be eliminated. This yields

$$\Phi_{i,k+1} - \Phi_{i,k} = (\mathrm{SPL}_{i,k+1} - \mathrm{SPL}_{i,k}) - 10\log_{10}(\Omega_{k+1}/\Omega_k)^{3+\alpha} = T_{i,k}, \quad i = 1,N, \quad k = 1,M-1 \tag{29}$$

Eqs. (22) and (29) constitute a new algebraic system of $N_{eq}=(M-1)N+\sum_{k-1}^{M-1} N_k$ linear equations in $N_{un}=M\times N$ unknown values of $\Phi_{i,k}$. The absence of Γ_i in the new system makes $\Phi_{i,k}$ independent of it and thus the trend of Γ_i cannot affect convergence and related errors. This is confirmed by the tests reported in 3.4.1. Γ_i is obtained by direct substitution of $\Phi_{i,k}$ in Eq. (21).

More equations than unknowns are likely to result since the spectra are typically measured at $M=5$ values of Ω (usually $\sum_{k=1}^{4} N_k > N$ and thus $N_{eq}=4N+\sum_{k=1}^{4} N_k > 5N = N_{un}$). The input data set is larger than what is necessary and the system is redundant, obliging to solve it by means of error minimization techniques. This is not a disadvantage since it improves the accuracy of the results. However, assuming that there are no experimental errors and that the numerical approximations due to the linear interpolation are negligible, a number of linearly dependent equations results and the intrinsic indeterminacy in the absolute levels of both Φ and Γ remains. Hence, after the spectral decomposition, the value of K will have to be imposed employing considerations based on the physics of the problem. This results in opposite shifts of Φ and Γ.

A further numerical problem arises: in Eq. (22) $\Phi_{i,1}$ appears only on the left-hand side while $\Phi_{i,M}$ appears only on the right-hand side. Thus, for any i the unknowns $\Phi_{i,1}$ and $\Phi_{i,M}$, relative to the extreme rotational speeds Ω_1 and Ω_M, are more weakly linked to the others than the unknowns $\Phi_{i,k}$ relative to the intermediate rotational speeds Ω_k, $k=2, M-1$ and lower accuracy of the solution may result. Hence, it is worth linking the unknowns relative to the same St and to Ω_1 and to Ω_M by means of an equation analogous to Eq. (22):

$$\Phi_{i,M}=b_{i,M}\Phi_{I,1}+c_{i,M}\Phi_{I+1,1}, \quad i=N_M,N \tag{30}$$

where $N_M=\mathrm{int}(\Omega_M/\Omega_1)$, $I=\mathrm{int}(i(\Omega_1/\Omega_M))$, $b_{i,M}=I+1-i(\Omega_1/\Omega_M)$, and $c_{i,M}=1-b_{i,M}$. This may be done only for those $\Phi_{i,k}$ ($k=1$ and M) for which the St ranges relative to Ω_1 and Ω_M overlap, that is for $i=N_M, N$. Eq. (30) and the other relations have been obtained from Eqs. (22)–(28) substituting M, 1, and 1 in place of k, $k+1$, and N, respectively. Again, if there are no experimental errors and if the numerical approximations due to the linear interpolation are negligible, Eq. (30) is dependent on the set resulting from Eq. (22) written for $k=1, M-1$. Thus, in principle, no new information is added but, as it will be seen in Section 3.3, an important improvement in the accuracy results.

The computed "free-field" SPL, $(\mathrm{SPL}_{comp})_{i,k}$ may be reconstructed solving Eq. (21) with respect to $\mathrm{SPL}_{i,k}$, substituting the computed $\Phi_{i,k}$, summing $10\log_{10}(\Omega_k^{3+\alpha})$ and assigning $\Gamma_i=0$. The value of C is implicitly included in the value of K, which, in the present work, is regarded as a constant to be assigned.

3.2. The solution algorithm

The system to be solved is constituted by Eqs. (29), (22), and (30) and its solution is given by the $N\times M$ values of $\Phi_{i,k}$ for $i=1, N$ and $k=1, M$. More precisely, M pieces of $\Phi(St)$ are obtained which are defined on M usually overlapping St ranges $St_{\min,k}$–$St_{\max,k}$. Each range depends on Ω_k since $St_{\min,k}=2\pi f_1/\Omega_k$ and $St_{\max,k}=2\pi f_N/\Omega_k$.

Once $\Phi_{i,k}$ has been found, $\Gamma_i=\Gamma(He_i)$, $i=1, N$, may be computed by direct substitution of $\Phi_{i,k}$ in Eq. (21). In fact, M pieces $\Gamma_{i,k}=\Gamma_k(He_i)$ defined over M perfectly superposed He ranges may be found. In principle these pieces should be coincident since Γ is independent of Ω but they are actually slightly different due to a number of reasons. Basically, experimental errors, errors in the computation of the power spectra, numerical approximations, and presence of parts of the measured power spectra which do not respect the structure of Eq. (10) may be a further reason of dispersion of the $\Gamma_k(He_i)$ trends. Obviously, it is more convenient to calculate a mean value $\overline{\Gamma}_i=1/M\sum_{k=1}^{M}\Gamma_{i,k}$ and to employ the dispersion of $\Gamma_{i,k}$ about $\overline{\Gamma}_i$ as an overall estimate of the accuracy and correctness of the results. Systematic experimental errors, function of f would be recognized by the algorithm as propagation effects and could not be identified in any way.

Due to the above listed reasons and since the number of equations N_{eq} will hardly equal the number of unknowns N_{un}, the system cannot be immediately solved. Thus, a new linear system with $N_{eq}=N_{un}$ will be found by means of the least squares method [14]; the latter method is well known and only the strictly necessary relations will be reported here. The general form of an algebraic linear system of $m=1, N_{eq}$ equations in the unknowns x_n, $n=1, N_{un}$ is

$$\sum_{n=1}^{N_{un}} a_{m,n}x_n=b_m, \quad m=1,N_{eq} \tag{31}$$

An approximate solution y_n satisfies the mth equation with an error

$$e_m=\sum_{n=1}^{N_{un}} a_{m,n}y_n-b_m, \quad m=1,N_{eq} \tag{32}$$

The norm E of the error is given by

$$E=\sqrt{\sum_{m=1}^{N_{eq}} e_m e_m}=\sqrt{\sum_{m=1}^{N_{eq}}\left[\left(\sum_{n=1}^{N_{un}} a_{m,n}y_n-b_m\right)\left(\sum_{j=1}^{N_{un}} a_{m,j}y_j-b_m\right)\right]} \tag{33}$$

$E=0$ if and only if $y_n=x_n$. For overdetermined systems an exact solution x_n does not exist thus $E>0$ always and only a "best" solution x_n^* may be found, the one which minimizes E. x_n^* is the solution of the N_{un} linear equations $(\partial E^2/\partial y_l)=0$, $l=1, N_{un}$

and this condition corresponds to

$$\sum_{n=1}^{N_{un}}\left(\sum_{m=1}^{N_{eq}} a_{m,l}a_{m,n}\right)x_n^* = \sum_{n=1}^{N_{un}} A_{l,n}x_n^* = B_l = \sum_{m=1}^{N_{eq}} a_{m,l}b_m, \quad l=1,N_{un} \tag{34}$$

The system to be solved has the form $\sum_{n=1}^{N_{un}} A_{l,n}x_n^* = B_l$ where x_n^* corresponds to $\Phi_{i,k}$. $A_{l,n}$ and B_l (n, l=1, N_{un}) must be found from $a_{m,n}$ and b_m, which may be obtained from Eqs. (29), (22), and (30). Some of $a_{m,n}$ correspond to the coefficients of the unknown $\Phi_{i,k}$ but most of them equal zero, resulting in a sparse coefficients matrix. Part of b_m equal $T_{i,k}$, the right-hand side term of Eq. (29), and the remainder are zero since Eqs. (22) and (30) are homogeneous in $\Phi_{i,k}$. Finding the correspondence between the coefficients requires establishing the correspondence between the subscripts m and n of Eq. (31) and the subscripts i, I, and k of Eqs. (29), (22), and (30). Once $a_{m,n}$ and b_m have been found, $A_{l,n}$ and B_l may be obtained from Eq. (34): $A_{l,n} = \sum_{m=1}^{N_{eq}} a_{m,l}a_{m,n}$ and $B_l = \sum_{m=1}^{N_{eq}} a_{m,l}b_m$. The bi-conjugate gradient method, [14], will be used to solve such a large algebraic linear system.

The sparseness of the coefficients matrix of the system given by Eq. (34) allows a fast solution of the system, but requires an efficient indexing of the non-zero terms. In turn this requires a detailed knowledge of the structure of the coefficients matrix of the system given by Eq. (31). The description of the latter is surely worthy and will be given hereinafter. On the contrary, due to the more complex structure of the coefficients matrix of the system given by Eq. (34), the positions of its non-zero elements will not be given.

The basic structure of the system given by Eq. (31) is shown in Fig. 1. The coefficients matrix has n=1, N_{un} columns, with N_{un}=NM and n=[k+(i−1)M] (that is $x_1^* = \Phi_{1,1}$, $x_M^* = \Phi_{1,M}$, $x_{M+1}^* = \Phi_{2,1}$, etc.). The coefficients matrix is composed of the following:

(1) An upper part derived from Eq. (29) which contains N blocks, Fig. 2a, of $M-1$ rows and M columns, resulting in m=1, $N\times(M-1)$ rows. Each row is related to a pair Ω_k and Ω_{k+1}, k=1, $M-1$ and each block is related to a frequency value f_i, i=1, N. The mth row, m=[k+(i−1)(M−1)], contains the two non-zero elements – 1 and 1 in the columns n=[k+(i−1)M] and n=[k+(i−1)M+1], respectively.

(2) A lower part derived from Eqs. (22) and (30) and containing a total number of $\sum_{k=1}^{M} N_k$ rows for m=[$N\times(M-1)$+1], [$N\times(M-1)+\sum_{k=1}^{M} N_k$]. The rows derived from Eq. (22), Fig. 2b, and from Eq. (30), Fig. 2c, have three non-zero elements per row; an element equals 1 and is located in the [k+(i−1)$\times M$]th column. In the rows derived from Eq. (22) the other non-zero elements are located in the [k+1+(I−1)$\times M$]th and in the [k+1+I$\times M$]th columns and equal – $b_{i,k}$ and – $c_{i,k}$, respectively. In the rows derived from Eq. (30) the other non-zero elements equal $-b_{i,M}$ and $-c_{i,M}$ and are located in the [1+(I−1)$\times M$]th and in the [1+I−M]th columns, respectively. In both cases I is obtained substituting the actual value of k in Eq. (25).

The right-hand side vector is composed of two parts corresponding to the upper and lower parts of the coefficients matrix. In the upper part there are the elements b_m, m=1, $N\times(M-1)$ which equal $T_{i,k}$, Eq. (29), and are usually non-zero. All the elements in the lower part equal zero since they derive from Eqs. (22) and (30), which are homogeneous in the unknown Φ.

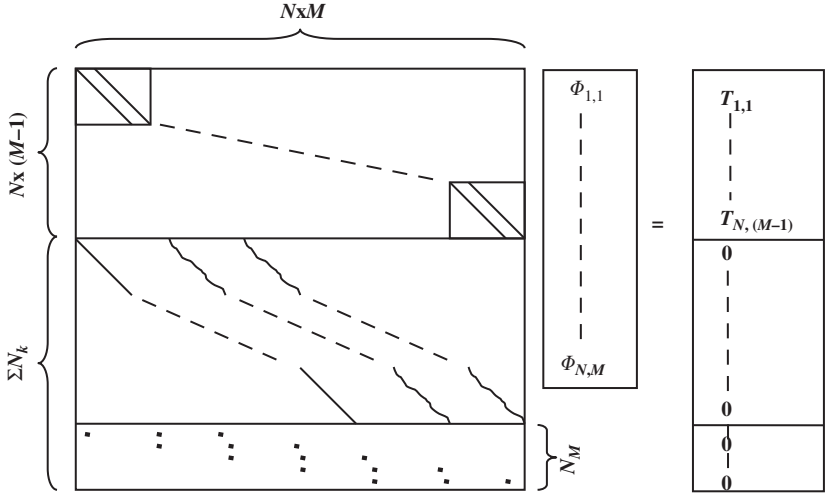

Fig. 1. Structure of the system derived from Eq. (31).

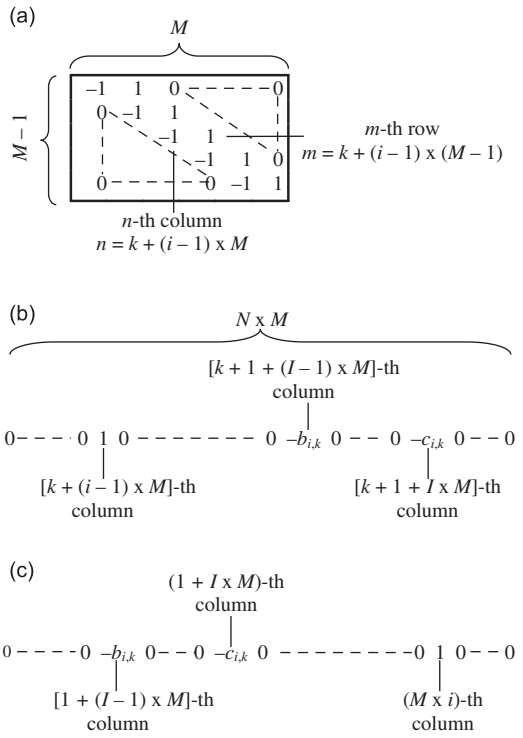

Fig. 2. System derived from Eq. (31): (a) Upper block derived from Eq. (29). (b) Row derived from Eq. (22). (c) Row derived from Eq. (30).

3.3. Accuracy of the method

This section is aimed at providing some guidelines for the choice of the ranges and spacings of both f and Ω. To this purpose, the solution of the linear system resulting from Eqs. (22), (29), and (30) should be considered as composed of two steps:

(1) Solution of Eq. (29) at He=const (i.e. at i=const). One arbitrarily assigns $\Phi_{i,1}$ and directly obtains $\Phi_{i,k}$ for k=2, M within the St range $St_{i,1}$–$St_{i,M}$, i.e. $2\pi f_i/\Omega_1 - 2\pi f_i/\Omega_M$. This is correct no matter the values of both $\Delta\Omega$ and Δf. Letting i vary between 1 and N yields N pieces of M values of the function Φ, defined over N different St ranges. Usually, the N pieces do not superpose due the arbitrary choice of $\Phi_{i,1}$, i=1, N and thus they must be matched with each other.

(2) Shift and superposition of the N pieces of Φ in the y-axis direction, as seen in Section 2.2. To do this properly, it is necessary that the Φ pieces relative to neighboring frequency (i.e. He) values present a sufficient overlap, which requires a sufficient overlap in the related St ranges. Unfortunately, it is possible that this does not happen, resulting in the most serious cause of inaccuracy of the procedure. The overlap of the St ranges depends on the spacings Δf and $\Delta\Omega$ and on the ranges f_1–f_N and Ω_1–Ω_M. In principle, to match the Φ pieces it is sufficient to find a relation between the N arbitrarily chosen $\Phi_{i,1}$ but in practice the variable St spacing and the data spreading due to the experimental errors make the shift of the N Φ pieces more precise if it is done by means of Eqs. (22) and (30) which link most of $\Phi_{i,k}$ and not only the N arbitrary $\Phi_{i,1}$. Obviously, a large number of Φ values within each Φ piece (i.e. a large M value) surely improves the accuracy of the shift procedure.

The condition on the St ranges overlap may be analyzed considering inequality (23) and Eq. (25) with the purpose of obtaining a well-conditioned coefficients matrix. To this aim, Eqs. (22) and (30) must be independent of Eq. (29). First, let us consider how such a problem arises with Eq. (22). For fixed values of i and k, Eq. (29) links $\Phi_{i,k}$ and $\Phi_{i,k+1}$ only and thus, in order to avoid duplicating this link, Eq. (22) should not contain $\Phi_{i,k+1}$. It links $\Phi_{i,k}$, $\Phi_{I,k+1}$, and $\Phi_{I+1,k+1}$ and thus the resulting condition is $I \geq i+1$ for all values of i and k, which means that $St_{I,k} \geq St_{i+1,k}$, i.e. $f_I \geq f_{i+1}$. In case I=i, the interpolation of Eq. (22) becomes an extrapolation of the trend between $\Phi_{i,k}$ and $\Phi_{i,k+1}$ and the situation becomes even more severe if the coefficient $c_{i,k}$ of Eq. (27) is small. In the latter case the coefficient $b_{i,k}$ of Eq. (26) approaches 1, a weak coupling of $\Phi_{i,k}$ with unknowns other than $\Phi_{i,k+1}$ results and the system may degenerate. The least square method and the bi-conjugate gradient method are very robust and the whole algorithm can hardly diverge but, obviously, there may be errors in those parts of the solution where I=i. However, the overall loss of accuracy is also related to the number of points at which I=i.

Considering Eq. (25), the condition $I \geq i+1$ becomes $I = \mathrm{int}(i(\Omega_{k+1}/\Omega_k)) \geq i+1$ thus yielding

$$i \geq \frac{\Omega_k}{(\Omega_{k+1}-\Omega_k)} = \frac{\Omega_k}{\Delta\Omega} \tag{35}$$

Therefore $\Delta\Omega$ must not be too small in comparison with Ω_k. This condition is to be respected for any Ω_k, $k=1, M-1$ and hence it must be applied to the most unfavorable situation, i.e. for $k=M-1$, where Ω is maximum. This yields $i \geq \Omega_{M-1}/\Delta\Omega$, which, considering Eq. (18), results in $f \geq \Omega_{M-1}\Delta f/\Delta\Omega$.

Eq. (30) yields a less restrictive condition: to avoid decoupling, $\Phi_{1,1}$, the value at the lowest frequency, for which the situation is most severe, must be present in at least one of the resulting equations and has to be linked to a value of $\Phi_{i,M}$ at any frequency $f_i \geq f_2$. In other terms, there must exist $i \geq 2$ such that Eq. (30) yields $I=1$. That is $I = \mathrm{int}(i(\Omega_1/\Omega_M)) = 1$, which results in

$$1 + \frac{\Omega_M}{\Omega_1} \geq i \geq \frac{\Omega_M}{\Omega_1} \tag{36}$$

which is more easily respected than inequality (35). This proves the usefulness of Eq. (30).

However, inequalities (35) and (36) are sufficient rather than necessary conditions to avoid the data decoupling. Indeed, if the linear interpolation is adequate for the local characteristics of the experimental data set (basically their smoothness, slope, and curvature) the accuracy may not be as affected as it could be expected simply based on the reported analysis.

Inequalities (35) and (36) represent the condition to avoid data decoupling at low frequencies but a similar, though less severe, loss of accuracy may take place at high frequencies too. It is due to the incomplete superposition of the St ranges ($St_{\min,k}$–$St_{\max,k}$) related to the different Ω_k at which the SPL spectra have been measured. At Ω_M the St range upper bound is $St_{\max,M}=2\pi f_{\max}/\Omega_M$ and is the smallest one (i.e. $St_{\max,k}=2\pi f_{\max,k}/\Omega_k > St_{\max,M}$ for any $k<M$). Thus for $St < St_{\max,M}$ data at $St=const$ are available in all of the M spectra while for $St > St_{\max,2}=2\pi f_{\max}/\Omega_2$ such data are available only at $\Omega=\Omega_1$. In the intermediate cases, i.e. for $St_{\max,2} < St < St_{\max,M}$, data are available in a number of spectra varying between 2 and $M-1$. As a result, the number of spectra to which Eq. (22) may be applied gradually decreases as St becomes larger than $St_{\max,M}$ and the overall accuracy decreases too. Anyway, Eq. (30) may be employed up to $f=f_{\max}$ and thus the unknowns $\Phi_{i,k}$ at $St > St_{\max,M}$ are not completely decoupled from the ones at $St < St_{\max,M}$. Therefore, this is not expected to be a severe problem, but it is worthy that all SPL spectra provide data in the St range of interest, i.e. that the upper bound of this range is smaller than $St_{\max,2}$ at least, thus requiring a suitable choice of the f and Ω ranges.

3.4. Effect of the typical features of measured spectra on the performance of the algorithm

The present section is aimed at verifying how the results of the method may be affected by ranges and spacings of both f and Ω. The effect of experimental errors is considered too. Determination and correctness of α and K are not concerned since in the present work their values have to be assigned. The algorithm has been implemented in a Fortran program which has been tested using data numerically generated according to a simplified form of Eq. (11):

$$\mathrm{SPL}_{\mathrm{prop,an}}(f,n) = \mathrm{SPL}_{\mathrm{ff,an}}(f,n) + \Gamma_{\mathrm{an}}(He) \tag{37}$$

$\mathrm{SPL}_{\mathrm{ff,an}}$ is the "free-field SPL", the quantity without undesired propagation effects, and $\mathrm{SPL}_{\mathrm{prop,an}}$ is the SPL in presence of propagation effects. For easiness, in these tests the rotational speed $n=60\ \Omega/2\pi$ (rev/min) is used instead of Ω (rad/s). $\mathrm{SPL}_{\mathrm{ff,an}}$ is given by

$$\mathrm{SPL}_{\mathrm{ff,an}}(f,n) = \Phi_{\mathrm{an}}(St) + 10\log_{10} n^{3+\alpha} - 50 \tag{38}$$

with $\alpha=1$. Φ_{an} and Γ_{an} are computed by means of the following analytical expressions:

$$\Phi_{\mathrm{an}}(St) = 10\log_{10}\frac{(St/50)^4}{[1+(St/50)^4]^2} \tag{39}$$

$$\Gamma_{\mathrm{an}}(He) = 10\log_{10}[1-0.95\sin(\gamma He)] \tag{40}$$

where f is expressed in Hz, $St=60\,f/n$, and $He=f/1046$. The parameter γ acts on the "frequency period" of the peaks of Γ, thus allowing to represent operation in free-field conditions ($\gamma=0$) or in strongly reflecting environment ($\gamma>0$). The trend of $\mathrm{SPL}_{\mathrm{prop,an}}$ resulting from Eq. (37) is typical of the trailing edge noise generated by open rotors of axial flow fans.

To evaluate the accuracy of the method, one may compare $\mathrm{SPL}_{\mathrm{comp}}$, the free-field SPL spectrum reconstructed by means of the spectral decomposition, with $\mathrm{SPL}_{\mathrm{ff,an}}$. To this aim the difference (error) between $\mathrm{SPL}_{\mathrm{comp}}$ and $\mathrm{SPL}_{\mathrm{ff,an}}$ is employed:

$$e_{\mathrm{SPL}}(f,n) = \mathrm{SPL}_{\mathrm{comp}}(f,n) - \mathrm{SPL}_{\mathrm{ff,an}}(f,n) \tag{41}$$

Due to Eqs. (37) and (38) and to the use of Eq. (21) for reconstructing $\mathrm{SPL}_{\mathrm{comp}}$, the equality $e_\Phi = -e_\Gamma = e_{\mathrm{SPL}} + \mathrm{const}$ results. Hence, to evaluate the correctness of the results it is sufficient to study the trend of e_{SPL}. In all computations, the assigned α equals 1, i.e. the value employed in Eq. (38). Since in the present work K is an arbitrary constant, the absolute levels are not important and a constant e_{SPL} indicates that the exact Φ has been obtained. A variable trend indicates the presence of errors.

Some preliminary tests have shown that the method may converge even with spectra related to $M=2$ values of Ω only, but further tests with superposed random errors have shown that $M=5$ is a good trade-off between accuracy and size of the input data set. Thus, $M=5$ has been assumed as standard value. The reported tests show that the method works properly and that it may be employed to perform the spectral decomposition of experimental SPL power spectra. This issue will be confirmed by the practical application shown in the next chapter.

3.4.1. *Effect of the propagation function and general features of the solution*

To study the effect of Γ on the solution, the values 0.2, 2, 40 have been considered for γ, yielding a "frequency period" of 32,861, 3286, and 164.5 Hz, respectively. $M=5$ rotational speeds have been employed with $\Delta n=500$ rev/min, resulting in $n=2000$, 2500, 3000, 3500, and 4000 rev/min. The spectra, Fig. 3, have been computed with $\Delta f=12.5$ Hz within the range 12.5–20,000 Hz.

After the spectral decomposition, a constant value of K has been subtracted from the computed spectra and its value has been chosen so as to superpose SPL_{comp} to $SPL_{ff,an}$ that is to minimize e_{SPL}. The absolute value of e_{SPL} is plotted in Fig. 4, for all of three cases, the trends are very similar and are almost independent of γ, thus confirming the comment to Eq. (29), i.e. that the absence of Γ from the system of equations makes Φ_{comp} independent of Γ_{an}. $|e_{SPL}|$ has some oscillations and a relatively large magnitude (1 dB at most) at $f<100$ Hz ($i<8$), then it quickly decreases of almost two orders of magnitude ($f=200$–1000 Hz) and finally it slightly grows for $f>1000$ Hz. The oscillations at low frequency are probably due to the decoupling between data at different frequencies described in Section 3.3. Indeed, the frequency ranges for the data decoupling resulting from inequalities (35) and (36) are similar to the ones where the oscillations take place: inequality (35) yields $i\geq(4000\text{ rev/min})/(500\text{ rev/min})=8$ ($f\geq 100$ Hz), while inequality (36) yields $i\geq(4000\text{ rev/min})/(2000\text{ rev/min})=2$ ($f\geq 25$ Hz). Thus at $i=1$ ($f=12.5$ Hz) the decoupling between data is complete, at $7\geq i\geq 2$ (87.5 Hz $\geq f\geq$ 25 Hz) the decoupling is partial, and above $i=7$ all the data are correctly coupled with each other. As reported in Section 3.3, the slight growth at high f is probably due to the fewer data available at the higher St. For each γ value, the very good superposition of the $|e_{SPL}|$ curves related to all n indicates that the computed Φ and Γ curves, not shown for reasons of space, collapse correctly on single curves too. Thus the algorithm does not add unexpected errors and works properly.

3.4.2. *Effect of the presence of random errors*

It is important to verify how much the random errors, which are always present in experimental data, affect Φ_{comp}. To this aim, fifteen independent random noise signals $S_{random}(f)$ have been numerically generated and then added to the $SPL_{prop,an}$ employed in the previous tests, thus yielding three data sets comparable to measured SPL power spectra. The fifteen $S_{random}(f)$ have the same statistical properties: they lie in the range ± 4 dB with a zero average and an rms of about 2.6 dB. Comparing with typical

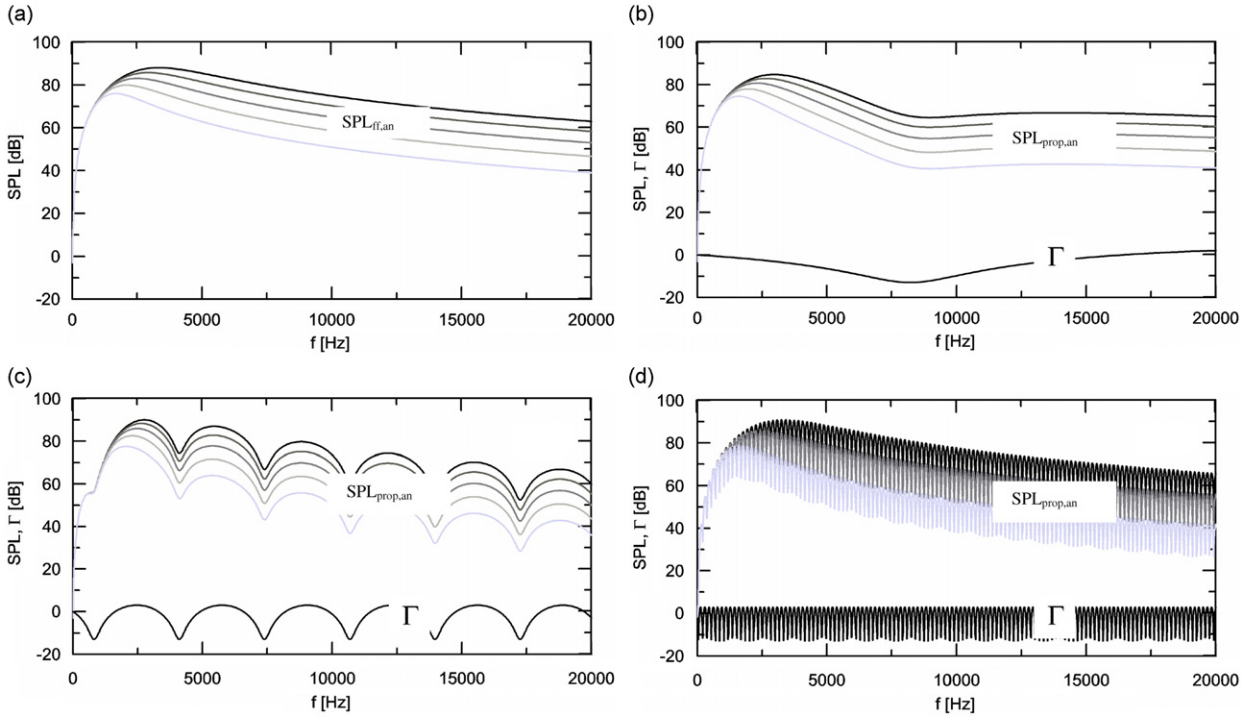

Fig. 3. SPL and Γ generated by means of Eqs. ((37)–(40)): (a) $SPL_{ff,an}$, $\gamma=0$. (b) $SPL_{prop,an}$, $\gamma=0.2$. (c) $SPL_{prop,an}$, $\gamma=2$. (d) $SPL_{prop,an}$, $\gamma=40$. — $n=2000$ rev/min; — $n=2500$ rev/min; — $n=3000$ rev/min; — $n=3500$ rev/min; – $n=4000$ rev/min.

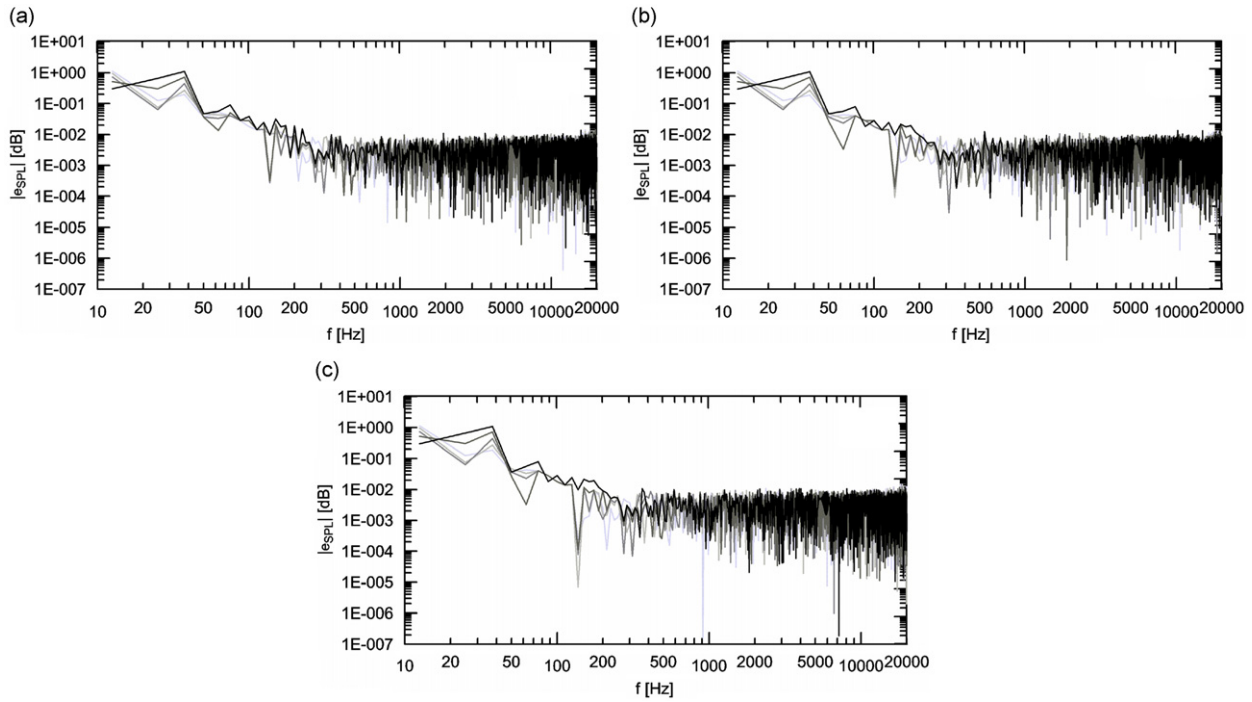

Fig. 4. Error in reconstructing $SPL_{ff,an}$: (a) $|e_{SPL}|$, $\gamma=0.2$. (b) $|e_{SPL}|$, $\gamma=2$. (c) $|e_{SPL}|$, $\gamma=40$. — $n=2000$ rev/min; — $n=2500$ rev/min; — $n=3000$ rev/min; — $n=3500$ rev/min; – $n=4000$ rev/min.

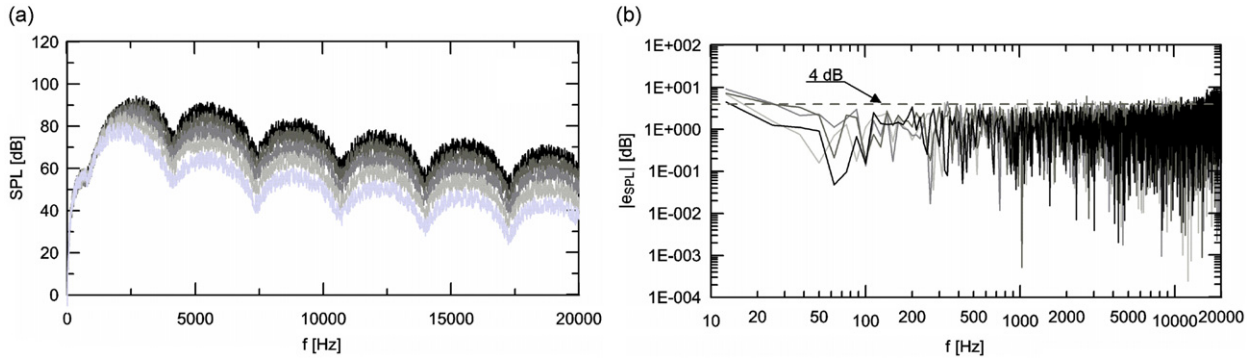

Fig. 5. Tests with random errors: (a) $SPL_{real,an}$. (b) $|e_{SPL}|$. — $n=2000$ rev/min; — $n=2500$ rev/min; — $n=3000$ rev/min; — $n=3500$ rev/min; – $n=4000$ rev/min.

experimental data, these are rather high values since a suitable choice of measurement parameters usually results in much smoother spectra. Anyway, this choice allows to visualize the results and to test the method under conditions more severe than the usual ones. The tests have been performed for the three cases $\gamma=0.2$, 2, and 40. Again, the computations have confirmed that Φ_{comp} is independent of Γ and thus, for reasons of space, only the plots relative to $\gamma=2$ are reported.

The important quantities are $SPL_{ff,an}$, resulting from Eq. (38), and $SPL_{real,an}$, the "realistic" quantity, representing the measured SPL, i.e. $SPL_{prop,an}$ with superposed random errors: $SPL_{real,an}=SPL_{ff,an}+\Gamma_{an}+S_{random}$. The chosen K minimizes the mean level of e_{SPL} and thus comparing e_{SPL} with the maximum level of S_{random} (4 dB) allows to evaluate how much the random errors affect the whole procedure. The plots of $SPL_{real,an}$ and $|e_{SPL}|$ are reported in Fig. 5. The irregular trend of $|e_{SPL}|$ indicates that, although the algorithm is based on an error minimization technique, the random fluctuations are not eliminated. Up to 10 kHz they are reduced (their level is smaller than 4 dB) and above 10 kHz they are slightly amplified (their level reaches about 10 dB at 20 kHz); this growth is probably caused by the fewer data available at high St, as mentioned in Section 3.3. However, the rms of e_{SPL} (between 2.15 dB, $n=4000$ rev/min, and 2.34 dB, $n=2000$ rev/min) is smaller than 2.6 dB, the rms of S_{random}.

At all n, the $|e_{SPL}|$ curves are well superposed with each other, indicating that the trends of SPL_{comp} correctly reproduce the original trends of $SPL_{ff,an}$. Despite the high level of S_{random}, the algorithm damps or at least does not excessively amplify the random errors, providing an indication of its robustness and accuracy.

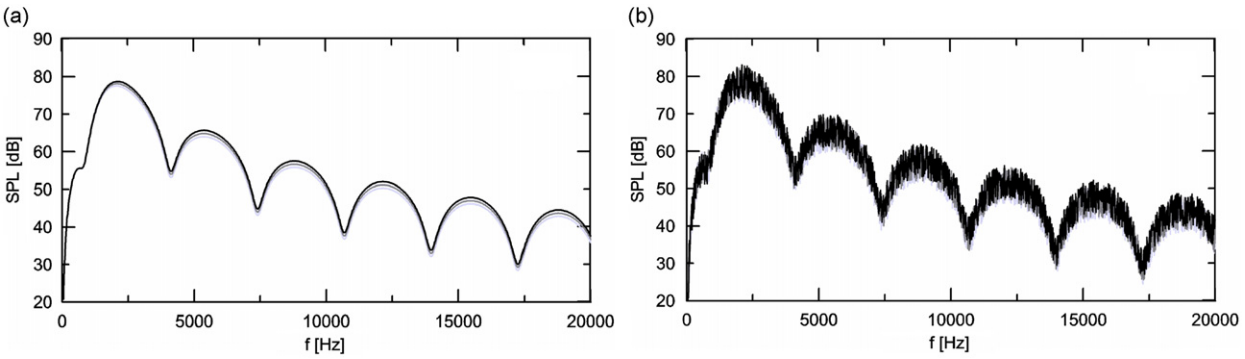

Fig. 6. SPL_{an} with reduced $\Delta\Omega$: (a) $SPL_{prop,an}$. (b) $SPL_{real,an}$. —n=2000 rev/min;– n=2050 rev/min;– n=2100 rev/min.

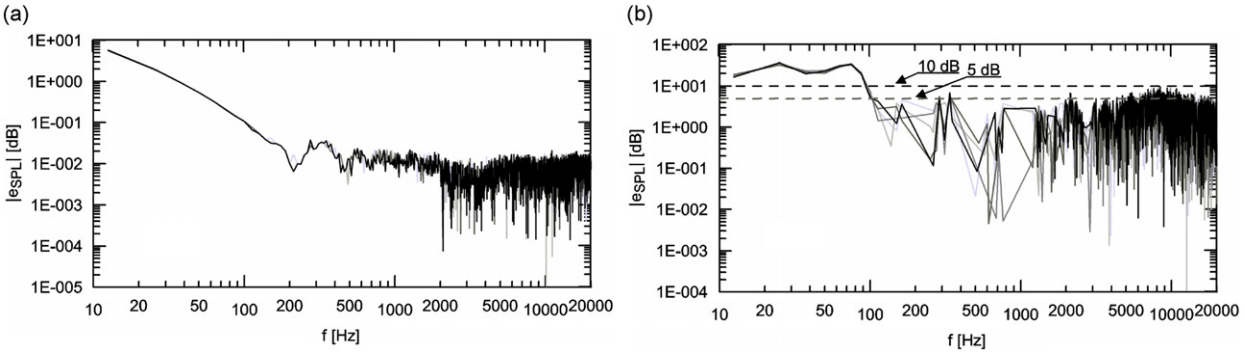

Fig. 7. Error in reconstructing $SPL_{ff,an}$ with reduced $\Delta\Omega$: (a) $|e_{SPL}|$ without random errors. (b) $|e_{SPL}|$ with random errors. — n=2000 rev/min; — n=2025 rev/min; — n=2050 rev/min; — n=2075 rev/min; – n=2100 rev/min.

3.4.3. *Effect of the rotational speed spacing*

In order to evaluate the effect of a reduced Δn, the tests have been repeated with Δn=25 rev/min, a very small, unrealistic value resulting in n=2000, 2025, 2050, 2075, and 2100 rev/min. Inequalities (35) and (36) show that complete coupling exists for $i \geq$ (2100 rev/min)/(25 rev/min)=84 ($f \geq$ 1050 Hz) and that weak coupling exists for $i \geq$ (2100 rev/min)/(2000 rev/min)=1.05, ($i \geq 2$ and $f \geq$ 25 Hz), respectively.

The input spectra, with and without random errors, Fig. 6, have been computed with γ=2 and Δf=12.5 Hz, within the range 12.5–20,000 Hz. The extremely small Δn results in a difference in the $SPL_{ff,an}$ curves of 2 dB at most, less than 2.6 dB, the rms of S_{random}. Such a condition is very unfavorable from the numerical point of view and is a further reason of severity for the tests in presence of random errors.

$|e_{SPL}|$ in absence of random error, Fig. 7a, has a maximum value of about 6 dB at f=12.5 Hz and quickly decreases to values smaller than 0.1 dB for $i \geq 7$, i.e. $f \geq$ 87.5 Hz (again, the chosen K minimizes the mean level of e_{SPL}). In the tests with random error, the value of K has been chosen to have the best superposition of SPL_{comp} and $SPL_{ff,an}$ for $f \geq$ 10 kHz, where the trend of the latter is correctly reproduced (i.e. where e_{SPL} is minimum). The $|e_{SPL}|$ plot, Fig. 7b, shows that the algorithm is able to extract the overall trend of $SPL_{ff,an}$ although important errors (10 dB or more) are present for $f \leq$ 10 kHz. Levels between 20 and 36 dB are present for $f \leq$ 87.5 Hz, where the decoupling between data is complete, while for $f \geq$ 10 kHz $|e_{SPL}|$ is smaller than 5 dB, a good result comparing with 4 dB, the maximum level of S_{random}. In the intermediate frequency range, e_{SPL} approximately lies in the range $\pm$10 dB. These tests, performed in rather severe and unrealistic conditions, provide a further indication of the robustness of the method.

4. A practical application of the method

The present chapter aims at showing the kind of results and information which may be obtained by means of the method and at verifying the practical difficulties in its application. There is no aim at studying any specific physical phenomenon and although it is not the main purpose of the present work, the criteria for estimating α and K presented in Section 2.1 will be applied and discussed. The discussion cannot prove that the assigned α and K are the actual ones, but it provides a physical ground for evaluating the correctness of the chosen values. Obviously, if the assigned values are not correct also the resulting Φ_{comp}, Γ_{comp}, and SPL_{comp} will not be the actual ones.

4.1. Description of the experimental setup and of the measured SPL

In order to obtain the experimental data sets, an axial flow fan for automotive use has been tested in the DIMSET hemi-anechoic chamber. The fan rotor has 7 blades and a tip diameter of 315 mm and has been provided by Johnson Electric—GATE. It has been mounted on a test plenum designed according to the ISO 10,302 prescriptions [15] with the rotational axis parallel to the floor at a height of 1 m and it has been operated at the design conditions (φ=0.164, $\psi = 8(p_{out}-p_0)/\rho_0(\Omega D)^2 = 0.104$).

The measurements have been taken by means of a Brüel & Kjær 3560 spectrum analyzer at M=5 different rotational speeds (n=2000, 2500, 3000, 3500, and 4000 rev/min) with the microphone placed on the rotational axis 1 m upstream of the runner. The SPL power spectra have been computed in the range 0–20 kHz with Δf=12.5 Hz employing 100 records of 1600 data weighted with a Hanning window (50% superposition). For such kind of measurements this typically results in errors of less than 1 dB in the SPL spectra computation. Two different configurations have been tested and the corresponding SPL spectra, before and after the spectral decomposition, have been compared. Since in both cases the generation mechanism is unchanged, the spectral decomposition is expected to result in the same Φ_{comp} and SPL_{comp} and in different Γ_{comp}. Assuming that the theory presented in Section 2.1 applies to the present cases, this allows to evaluate the effectiveness of the method.

The first configuration is a free-field one, constituted by the fan within the hemi-anechoic chamber in the standard test configuration; it is intended to approximate the ideal open rotor, for which $\Gamma(He)$=0 and the only propagation effect is represented by the term Ma^{α} of Eq. (9). In fact, slight propagation effects may be expected which are possibly due to reflections from the test plenum, diffraction and scattering by the rotor parts and non perfect anechoicity of the test environment. The second configuration has been obtained interposing a square wooden panel with a side 400 mm long between the fan and the microphone at a distance of 10 mm from the latter. This creates a strong, frequency dependent attenuation in the measured SPL, thus adding an important propagation effect to the free-field spectrum.

The spectra measured in the free-field configuration, $SPL_{ff,meas}$, Fig. 8a, have a typical trend: in the low f range ($f<3$–4 kHz) some peaks at the blade passing frequency harmonics (St=7, 14, 21, 28, and 35, i.e. below 2.4 kHz), thus due to the tonal noise, are superposed to rather uniform, slightly decreasing values. This trend probably results from the composition of the trailing edge noise with other kinds of noise, such as turbulence ingestion noise and noise due to the tip leakage flow. At the middle f (f=3.5–5.5 kHz), the spectrum has a change of slope resulting in an asymptotic trend at high f with a slope of about -3.4 (i.e. $S_{pp}(f)\overset{f\to\infty}{\longrightarrow} C/f^{3.4}$). This value is close to $-10/3$, the one found by Chase [13] for the trailing edge noise. Anyway, as far as the present procedure is concerned, the most interesting feature is the slightly wavy trend, apparent for $f>3.5$ kHz, which prevents from clearly identifying the shape of the spectrum. These "oscillations" have an amplitude of less than 2.5 dB and a "frequency period" of about 2.5 kHz. Their propagation nature may be inferred since in that frequency range the spectra relative to different n may be apparently superposed by means of a simple shift along the y-axis. This is the usual explanation for such a trend, Neise and Barsikow [2] and Mongeau et al. [4]. In principle, in absence of propagation effects, according to Eq. (14), the spectra should collapse on a single curve when scaled with $10\log_{10}(n/60)^{3+\alpha}$ and plotted versus St, thus allowing to estimate α. In the present case, basing on error minimization in matching the part of the spectra above St=14 (the 2nd blade passing frequency harmonic), the best collapse of the curves related to the free-field case results when α=0.7. The scaled curves are spread within a band of about 5 dB, Fig. 8b, and the propagation effects are expected to be the major cause for this. A confirmation of this fact may be found in the plots of SPL_{comp} and $\overline{\Gamma}_{comp}$, the SPL and Γ reconstructed by means of the spectral decomposition.

For $f<700$ Hz, the spectra measured in the shielded configuration, $SPL_{sh,meas}$, Fig. 9a are quite similar to the ones relative to the free-field configuration but for $f>700$ Hz, as the wavelength λ becomes smaller than the dimensions of the wooden panel, the differences between the two configurations become apparent and increase with f. The interposition of the wooden panel causes a strong wavy trend, clearly independent of n, as expected for such a propagation effect.

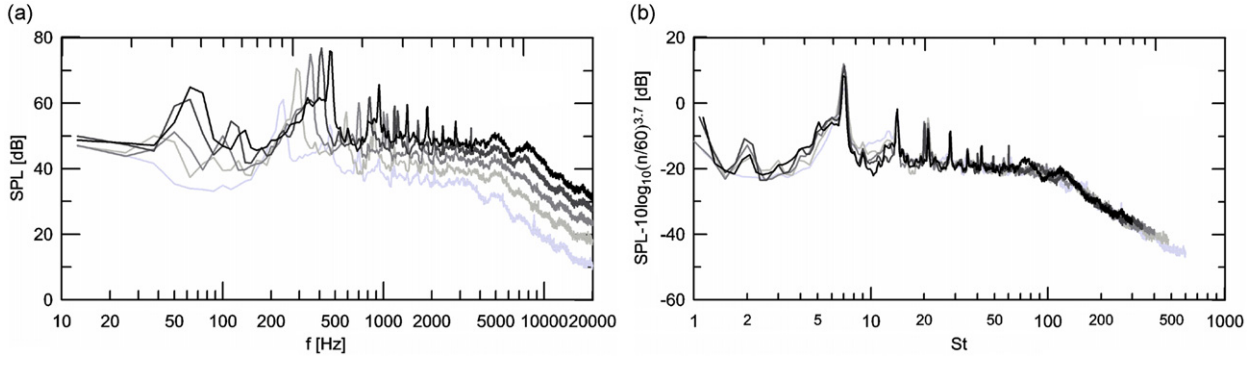

Fig. 8. $SPL_{ff,meas}$: (a) SPL versus f. (b) Scaled SPL versus St. — n=2000 rev/min; — n=2500 rev/min; — n=3000 rev/min; — n=3500 rev/min; – n=4000 rev/min.

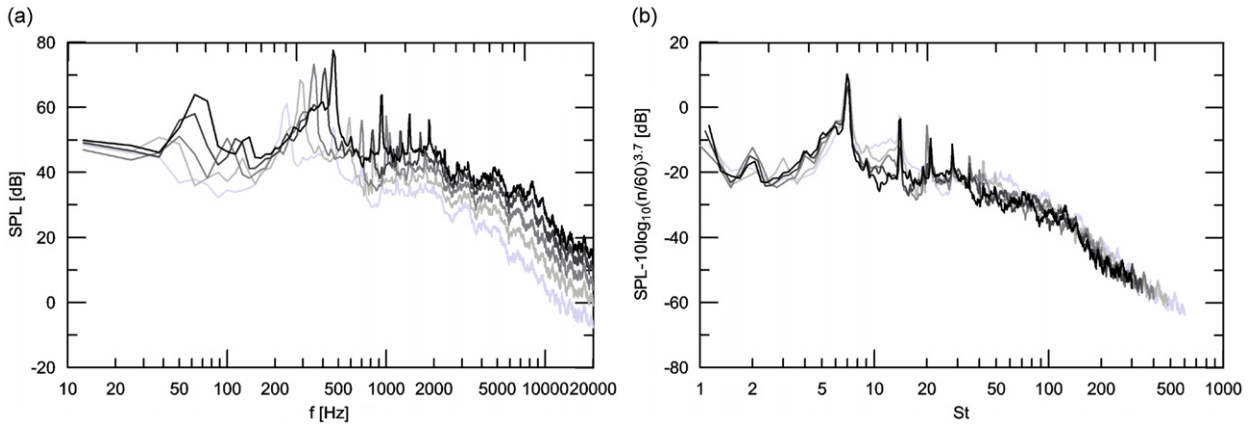

Fig. 9. $SPL_{sh,meas}$: (a) SPL versus f. (b) Scaled SPL versus St. — n=2000 rev/min; — n=2500 rev/min; — n=3000 rev/min; — n=3500 rev/min; – n=4000 rev/min.

The oscillations have an amplitude of about 5 dB with a rather constant "frequency period" (between 1.5 and 2 kHz) and, for $f>2$ kHz, a growing attenuation appears which reaches 15–20 dB at high f. The spectra, scaled with $10\log_{10}(n/60)^{3.7}$ and plotted versus St, Fig. 9b, collapse poorly due to a dispersion within a band of about 10 dB (the value α=0.7 has been chosen according to the scaling of the spectra measured in the free-field configuration). The propagation effects are again the expected cause for this dispersion.

4.2. Results of the spectral decomposition

Since α influences the asymptotic trends of both Φ and Γ, once the spectral decomposition has been performed, the analysis of the high f part of $SPL_{ff,comp}$ and $SPL_{sh,comp}$, Fig. 10a, and $\overline{\Gamma}_{ff,comp}$ and $\overline{\Gamma}_{sh,comp}$, Fig. 10b, may provide a check of the assigned value of α. Indeed, though chosen on a different ground, for $f>10$ kHz, the value 0.7 results in the flattest trend of $\overline{\Gamma}_{ff,comp}$ and in a constant mean value of $\overline{\Gamma}_{sh,comp}$. This agrees with the fact that, at high f, propagation phenomena are expected to be independent of f in the free-field configuration. Therefore, K_{ff} may be chosen imposing that $\overline{\Gamma}_{ff,comp}\cong 0$ $\overline{\Gamma}_{ff,comp}$ for $f>10$ kHz. The resulting levels and trends of $SPL_{ff,comp}$ and $SPL_{ff,meas}$ are very close, thus confirming the correctness of the assigned α and K_{ff}. K_{sh} may be found considering that the trends of both $SPL_{sh,comp}$ and $SPL_{ff,comp}$ should be almost identical since the source is the same and the propagation effects have been eliminated. To this aim, the $SPL_{sh,comp}$ curves have to be shifted as much as they can superpose to the $SPL_{ff,comp}$ ones.

Basing on the results of the tests described in Section 3.4, one may assume that, given a SPL data set respecting the structure of Eq. (10), the algorithm is able to separate the two parts Φ and Γ. Obviously, the numerically generated SPL employed in the tests fully respect the assumed structure but spectra computed from experimental data may be affected by inconsistencies of variable importance and origin. Due to the structure of the algorithm, Section 3.2, these inconsistencies would result in a dispersion of $\Gamma_{i,k}$ about its average $\overline{\Gamma}_i=(1/M)\sum_{k=1}^{M}\Gamma_{i,k}$. This dispersion may be evaluated by means of its rms value $\overline{e_\Gamma}$ (see Fig. 10c):

$$\overline{e_\Gamma}_i=\sqrt{\frac{1}{M}\sum_{k=1}^{M}(\Gamma_{i,k}-\overline{\Gamma}_i)^2} \tag{42}$$

The average value $\sum_{i=1}^{N}\overline{e_\Gamma}_i/N$ of $\overline{e_\Gamma}_i$ equals 0.380 dB in the free-field configuration and 0.342 dB in the shielded one.

The results of the application of the method, Fig. 10, may be analyzed with reference to three different frequency ranges:

- $f<80$ Hz, where the experimental errors are expected to strongly affect the results of the measurements and thus the results of the spectral decomposition cannot provide useful information.
- 80 Hz $<f<$ 700 Hz, where $SPL_{ff,comp}$ and $SPL_{sh,comp}$ should be identical and $\overline{\Gamma}_{ff,comp}$ and $\overline{\Gamma}_{sh,comp}$ are expected to be similar since the wooden screen dimensions (0.4 m) are smaller than λ (about 0.5–4 m).
- 700 Hz $<f<$ 20,000 Hz, where $SPL_{ff,comp}$ and $SPL_{sh,comp}$ should be identical while the differences between $\overline{\Gamma}_{ff,comp}$ and $\overline{\Gamma}_{sh,comp}$ are expected to grow with f due to the decrease of λ.

For $f<80$ Hz both $SPL_{ff,comp}$ and $SPL_{sh,comp}$ have similar trends but their levels differ of about 6 dB. On the contrary, $SPL_{ff,meas}$ and $SPL_{sh,meas}$ have more similar trends and levels, but in each case they are spread at random within a range of less than 4 dB. This dispersion is due to the experimental errors which are characteristic of measurements at such low f and are independent of n: locally, $SPL_{ff,meas}$ and $SPL_{sh,meas}$ do not respect the structure given by Eq. (10), resulting in the

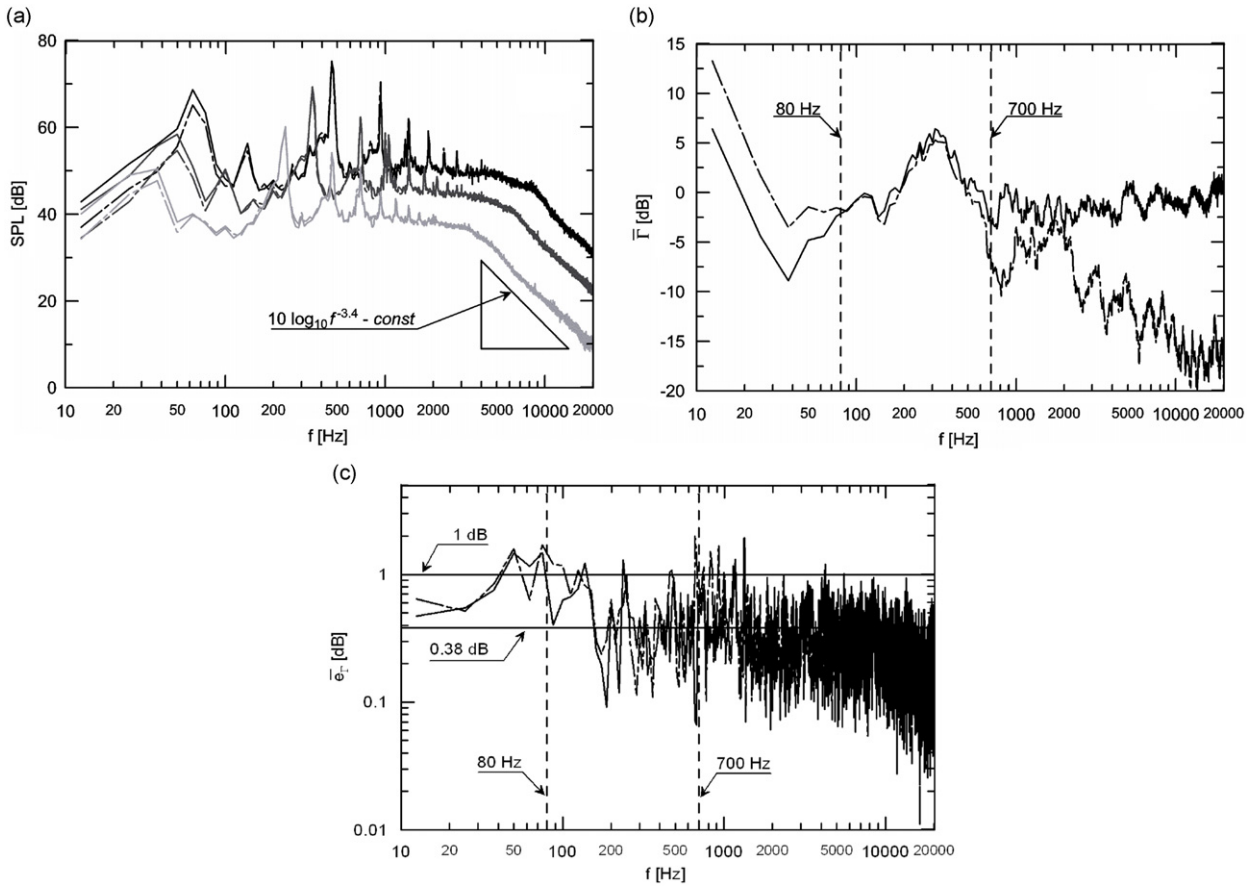

Fig. 10. SPL_{comp}, $\overline{\Gamma}$ and $\overline{e_\Gamma}$ in (—) free-field and (—·—) shielded configurations: (a) $SPL_{ff,comp}$ and $SPL_{sh,comp}$; —n=2000 rev/min; —n=3000 rev/min; –n=4000 rev/min. (b) $\overline{\Gamma}_{ff}$ and $\overline{\Gamma}_{sh}$. (c) $\overline{e_{\Gamma_{ff}}}$ and $\overline{e_{\Gamma_{sh}}}$.

observed differences in the SPL_{comp} curves. The same holds for both $\overline{\Gamma}_{ff,comp}$ and $\overline{\Gamma}_{sh,comp}$. $e_{\Gamma_{i,ff}}$ and $\overline{e_{\Gamma_{i,sh}}}$ are always larger than their rms values (0.380 and 0.342 dB, respectively) and attain values larger than 1 dB.

For 80 Hz $< f <$ 20,000 Hz both the $SPL_{ff,comp}$ and $SPL_{sh,comp}$ curves are quite similar to each other: the average difference between the curves related to the same Ω is smaller than 0.6 dB, in 10% of points it exceeds 1 dB and in 1.4% of points it exceeds 2 dB. These values are acceptable since they compare to the typical errors affecting the measured SPL spectra of present case. $SPL_{ff,comp}$ and $SPL_{sh,comp}$ are congruent with the expected trends: a wide flat part at the intermediate f (below 3–5 kHz, depending on n) and a smooth asymptotic trend proportional to $f^{-3.4}$ at high f. Below 700 Hz, the coincidence between $SPL_{ff,comp}$ and $SPL_{sh,comp}$ provides less information about the present algorithm since in that frequency range the $SPL_{ff,meas}$ and $SPL_{sh,meas}$ curves are rather close to each other. On the contrary, above 700 Hz, the spectra measured in the two configuration are apparently different and hence the good coincidence between $SPL_{ff,comp}$ and $SPL_{sh,comp}$ indicates that the method is able to identify their common generation mechanism.

For 80 Hz $< f <$ 700 Hz both $\overline{\Gamma}_{ff,comp}$ and $\overline{\Gamma}_{sh,comp}$ are quite similar to each other. This is in agreement with the fact that λ is larger than the wooden screen dimensions, resulting in a negligible effect on sound waves, i.e. in the same propagation effects for both configurations. For $f >$ 700 Hz $\overline{\Gamma}_{ff,comp}$ varies between -3 and 2 dB. $\overline{\Gamma}_{sh,comp}$ has a more complex trend: it oscillates between a minimum of about -10 dB at f=800 Hz and a maximum of -2.5 dB at f=1800 Hz; then an increasing attenuation takes place with oscillations in a range of about 7 dB. This trend agrees with the description of the measured spectra and may be attributed to the diffraction caused by the screen.

For $f >$ 80 Hz the trends of both $e_{\Gamma_{i,ff}}$ and $\overline{e_{\Gamma_{i,sh}}}$ present fluctuations generally below 1 dB, with a limited number of peaks not exceeding 2 dB for f=200–1500 Hz. These peaks are probably due to the tonal noise peaks in $SPL_{ff,meas}$ and $SPL_{sh,meas}$ at the blade passing frequency harmonics. Indeed, the tonal noise usually scales with Ma^3 while the whole spectrum has been scaled with $Ma^{0.7}$, thus resulting in a wrong scaling of the tonal noise component. This is expected to affect the spectral decomposition about the blade passing frequency and harmonics. However, the SPL data related to the tonal noise are very few comparing with the data related to the broad band noise and thus the former are not expected to affect the trends of Φ_{comp} and Γ_{comp}. Indeed, the typical magnitude of $\overline{e_{\Gamma_{i,ff}}}$ and $\overline{e_{\Gamma_{i,sh}}}$ compares to the random fluctuations of $SPL_{ff,meas}$ and $SPL_{sh,meas}$ indicating that the spectral decomposition should not be affected by other important sources of errors. Finally,

comparing the magnitude of $e_{\Gamma_{i,\mathrm{ff}}}$ and $\overline{e_{\Gamma_{i,\mathrm{sh}}}}$ with the typical variations of both $\overline{\Gamma}_{\mathrm{ff,comp}}$ and $\overline{\Gamma}_{\mathrm{sh,comp}}$ (5–7 dB) shows that, though not negligible, the errors cannot seriously affect the trends of the results.

This brief analysis shows that the present algorithm is able to recognize the common acoustic source in apparently different SPL spectra, separating the effect of the different measurement environment from the received noise. Furthermore, despite the limited number of employed spectra, the spectral decomposition is performed with errors which compare to the random errors affecting the measured spectra.

5. Conclusions

The application of the similarity theory to the aerodynamic noise generated by low Mach number sources such as low-speed fans has been presented with specific regard to the spectral structure of the SPL. Then, the spectral decomposition technique has been considered as a means of separating the noise part dependent on the flow velocity from the one due to propagation effects. Comparing with other existing works on the subject, the present study is specifically aimed at describing a data analysis technique together with its implementation. It is novel because of the following:

- The mathematical problem and the properties of its solution have been clearly analyzed.
- The developed algorithm is based on the rigorous solution of the derived equations. This has also allowed to analyze how typical measurement parameters may affect the accuracy of the method. A detailed description of the algorithm is reported too.

The main practical limitation of the method is the impossibility of determining absolute level and mean slope of the solutions. These indeterminancies are intrinsic to the physical phenomenon and thus they go beyond the main purpose of the present work. Nevertheless, some useful criteria for their estimate are suggested and applied.

The developed numerical algorithm has been carefully tested, with both measured noise signals and ad hoc numerically generated ones. These tests allow evaluating the robustness and effectiveness of the method and providing interesting information about the obtainable results. Furthermore, the method also allows to identify the noise generation mechanism of non-rotating aerodynamic sources whose noise power spectra scale with the flow velocity.

Acknowledgments

The authors kindly acknowledge Università di Genova for the financial support to the present work and Johnson Electric-GATE for providing the tested fan.

References

[1] J. Weidemann, Analysis of the relations between acoustic and aerodynamic parameters for a series of dimensionally similar centrifugal fan rotors, NASA Technical Translation NASA TT F-13-13, 798, 1971.
[2] W. Neise, B. Barsikow, Acoustic similarity laws for fan, *Journal of Engineering for Industry—Transactions of the ASME* 104 (1982) 162–168.
[3] L. Mongeau, D.E. Thompson, D.K. McLaughlin, Sound generation by rotating stall in centrifugal turbomachines, *Journal of Sound and Vibration* 163 (1993) 1–30.
[4] L. Mongeau, D.E. Thompson, D.K. McLaughlin, A method for characterizing aerodynamic sound sources in turbomachine, *Journal of Sound and Vibration* 181 (1995) 369–389.
[5] P.H. Bent, D.K. McLaughlin, Enhancements to noise source measurement techniques for turbomachinery, AIAA-Paper 93-4373, *15th AIAA Aeroacoustics Conference*, 1993.
[6] L.G. Tetu, D.E. Thompson, D.K. McLaughlin, Aeroacoustic similarity of centrifugal turbomachinery of different geometries, AIAA Paper 93-4371, *15th AIAA Aeroacoustics Conference*, 1993.
[7] L. Mongeau, D.A. Quinlan, An experimental study of broadband noise sources in small axial cooling fans, *Proceedings of the INCE Symposium on Fan Noise*, 1992, pp. 119–126.
[8] D.B. Stephens, S.C. Morris, A method for quantifying the acoustic transfer function of a ducted rotor, *Journal of Sound and Vibration* 313 (2008) 97–112.
[9] Z. Zhang, L. Mongeau, S.H. Frankel, Broadband sound generation by confined turbulent jets, *Journal of the Acoustical Society of America* 112 (2) (2002) 677–689.
[10] W.K. Blake, *Mechanics of Flow-Induced Sound and Vibration*, Academic Press, Inc., 1986.
[11] T.F. Brooks, D.S. Pope, M.A. Marcolini, Airfoil Self-noise and Prediction, NASA Reference Publication 1218, 1989.
[12] D.A. Quinlan, M.H. Krane, Aeroacoustic source identification using frequency dependent velocity scaling, AIAA Paper 1996-1743, *Second AIAA and CEAS Aeroacoustics Conference*, State College, Pennsylvania, May 6–8, 1996.
[13] D.M. Chase, Sound radiated by turbulent flow off a rigid half-plane as obtained from a wave vector spectrum of hydrodynamic pressure, *Journal of the Acoustical Society of America* 52 (2) (1972) 1011–1023.
[14] W.H. Press, S.A. Teukolski, W.T. Vetterling, B.P. Flannery, *Numerical Recipes*, Cambridge University Press, 1996.
[15] ISO 10302, Acoustics-method for the measurement of airborne noise emitted by small air-moving devices, 1996.